東北大学機関リポジトリ
TOUR
Tohoku University Repository

東北大学

Quantitative characterization of the fabrication processes of domain-inverted layers in LiTaO3 by the line-focus-beam ultrasonic material characterization system

Quantitative characterization of the fabrication processes of domain-inverted layers in LiTaO$_3$ by the line-focus-beam ultrasonic material characterization system

Masahito Miyashita and Jun-ichi Kushibiki[a)]
Department of Electrical Engineering, Tohoku University, Sendai 980-8579, Japan

Application of the line-focus-beam ultrasonic material characterization system was extended to evaluate Z-cut LiTaO$_3$ substrates with domain-inverted layers fabricated by proton exchange and quick heat treatment (QHT), and their fabrication processes and systems. Three Z-cut LiTaO$_3$ substrates were proton-exchanged at 260 °C for 20 min; heat-treated for 30 s at 520, 540, and 560 °C, with a temperature increase rate of 80 °C/s; and annealed at 420 °C for 6 h. Slab-type domain-inverted layers with 0.50, 1.94, and 3.26-μm depths on the $-Z$ surfaces and proton-exchanged layers on both the $-Z$ and $+Z$ surfaces were formed. Leaky surface acoustic wave (LSAW) velocities for both surfaces were measured in a frequency range of 100–300 MHz and found to exhibit different dispersion characteristics. Intrinsic LSAW velocity changes caused by the formation of domain-inverted layers were obtained from differences in the LSAW velocities for both surfaces. The velocity changes decreased with increases in the product fH of the ultrasonic frequency f and the domain-inverted layer thickness H. Relationships among the LSAW velocity changes, thicknesses of the domain-inverted layers, and process temperatures in QHT were experimentally obtained. An LSAW velocity variation of 2.6 m/s for the Y-axis propagation at 225 MHz was detected by a homogeneity evaluation on a specimen QHT-processed at 540 °C and annealed. This corresponded to a layer thickness variation of 0.20 μm and a QHT temperature variation of 2.9 °C. © *2002 American Institute of Physics.* [DOI: 10.1063/1.1504501]

I. INTRODUCTION

Domain-inverted layers are formed on LiNbO$_3$ and LiTaO$_3$ single-crystal substrates by Ti-diffusion[1,2] and heat-treatment just below the Curie temperature for LiNbO$_3$,[3] and by proton exchange[4] followed by heat treatment for LiTaO$_3$.[5,6] The physical constants in the domain-inverted layer, such as piezoelectric, pyroelectric, and electro-optic constants and optical nonlinear coefficients, which are associated with the direction of spontaneous polarization in the crystals, are opposite in sign to those of the substrate regions. Many devices have been researched and developed using the properties of domain-inversion, including bulk acoustic wave (BAW) and surface acoustic wave (SAW) devices, pyroelectric devices, and optical second-harmonic generation (SHG) and parametric oscillation devices.[3,5–15] The performance characteristics of the fabricated devices depend upon the fabrication process conditions. Domain-inverted structures and layer depths are usually evaluated by the chemical etching method.[16,17] However, this method has some disadvantages, such as time-consuming sample preparation, specimen destruction, and less accurate depth measurements.

We proposed the line-focus-beam ultrasonic material characterization (LFB-UMC) system[18,19] as a characterization and evaluation technology for proton-exchanged optical waveguides and their fabrication processes.[20–24] The elastic properties of materials can be evaluated and analyzed using the LFB-UMC system by measuring the propagation characteristics (phase velocity and propagation attenuation) of leaky SAWs (LSAWs) that propagate on specimen surfaces under the water-loaded condition. The usefulness of this ultrasonic method was successfully demonstrated in that the measurement resolutions of the depth and proton-exchanged conditions (time, temperature, and diffusion coefficient) were much higher than in conventional techniques.[21,24] Basic investigations into evaluating domain-inverted layers in Z-cut LiTaO$_3$ have also been reported by comparing the measured LSAW velocities with calculations using an ideal structural model.[22,23]

In this article, we define how to establish experimental procedures and collect basic data to apply the LFB-UMC system to evaluate domain-inverted layers in Z-cut LiTaO$_3$ fabricated by proton exchange followed by quick heat treatment (QHT) and the fabrication processes. We use the fabrication processes of domain-inverted layers for SHG devices using Z-cut LiTaO$_3$ single-crystal substrates.[12,13] Several specimens of Z-cut LiTaO$_3$ substrates with domain-inverted layers are fabricated under conditions with only the heat-treatment temperature varied. LSAW velocity measurements are conducted first. Next, domain structures and thicknesses are observed by the chemical etching method and depth profiles of the hydrogen and lithium ions in the substrates are analyzed by secondary-ion mass spectrometry (SIMS). The ultrasonic method of evaluating the domain-inverted layers and their fabrication process conditions are investigated and discussed here based on the obtained results.
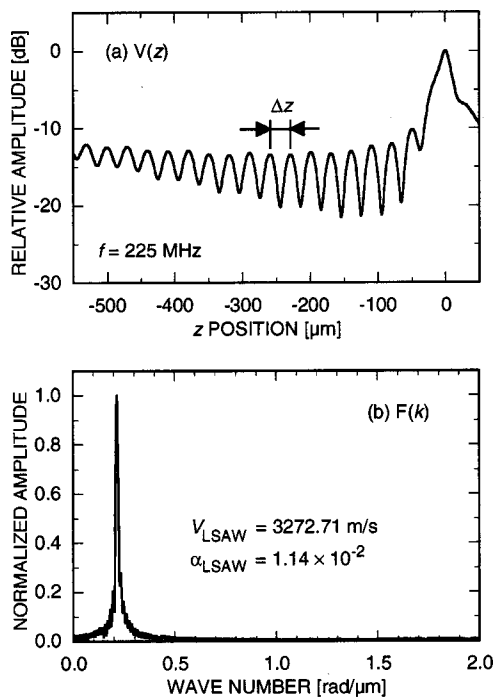
a)Electronic mail: kushi@ecei.tohoku.ac.jp

FIG. 1. Typical $V(z)$ curve (a) measured for a minus Z-cut Y-propagating LiTaO$_3$ substrate with a 1.94-μm-thick domain-inverted layer at 225 MHz and spectral distribution (b) analyzed by FFT for the $V(z)$ curve shown above.

II. LFB-UMC SYSTEM

The LFB-UMC system[18,19] is used to measure $V(z)$ curves. The measurement principle of the system is detailed in the literature.[18] The $V(z)$ curve is the transducer output obtained by changing the distance z between the ultrasonic device and the specimen surface. Figure 1 shows a typical $V(z)$ curve measured at 225 MHz for a minus Z-cut, Y-propagating (ZY) LiTaO$_3$ substrate with a domain-inverted layer 1.94-μm thick after the QHT process and the final results obtained by a fast Fourier transform (FFT). An oscillation interval Δz is obtained from $V(z)$ curve analysis. The LSAW velocity used for evaluation is obtained by substituting Δz into the following equation:

$$V_{\text{LSAW}} = \frac{V_W}{\sqrt{1 - \left(1 - \dfrac{V_W}{2\,f\Delta z}\right)^2}}, \qquad (1)$$

where V_W is the longitudinal wave velocity in water and f is the ultrasonic frequency. LSAW velocities may include measurement errors from the influence of the reflected waves from the specimen's back surface when the specimen is thin. Effective methods for removing the errors have been proposed.[25,26] An approximated method of obtaining the differences in LSAW velocities measured before and after the processes[21,22,24] was used in this article to avoid this problem.

III. SAMPLE PREPARATION

Three substrates cut from a 2 in. Z-cut LiTaO$_3$ wafer with both sides optically polished (optical grade, Yamaju Ceramics Co., Ltd., Seto, Japan), 13 mm (X)$\times$26 mm (Y) $\times$0.5 mm (Z), were employed for the experiments. All the specimens were first proton-exchanged at 260 °C for 20 min in a pyrophosphoric acid solution using an Al dry block bath and a 200-cm^3 SiO$_2$ glass beaker.[24] The three specimens were then heat-treated in air for 30 s at 520, 540, and 560 °C. This process is called QHT because of the very fast rising rate of 80 °C/s and the short soak time of 30 s using an infrared ray gold image furnace (RHL-P610CP, ULVAC-RIKO, Inc., Yokohama, Japan).[13] Ta thin films were sputtered with 30-nm thickness on all the $-Z$ surfaces of the specimens. The specimens with the $-Z$ surfaces upward were placed on a graphite plate 40 mm$\times$90 mm$\times$2 mm so the specimens could be efficiently heated and cracks prevented during the QHT process.[13] The Ta films were completely removed after the QHT process by immersing the specimens in a mixture of HF and HNO$_3$ (2:1 in volume) at 70 °C for about 20 s. We confirmed that there were neither roughness nor cracks on either surface of the specimens by an optical microscope. Finally, all the specimens were annealed in air at 420 °C for 6 h using the infrared ray furnace. Annealing is a necessary process for fabricating SHG devices and plays an important role in reducing optical loss in optical waveguides fabricated by proton exchange.[12] The specimens were sandwiched between two thin graphite plates in the annealing process, and the interval from room temperature to 420 °C was 1 min. The specimens and graphite plates were naturally cooled after the heat treatment in both the QHT and annealing processes. Domain-inverted layers with depths of a few microns were formed on all the $-Z$ surfaces of the specimens by the QHT process,[5,12,13] and proton-diffused layers were formed on both the $-Z$ and $+Z$ surfaces of the specimens by the series of proton exchange, QHT, and annealing processes,[22] as will be confirmed and discussed later.

IV. EXPERIMENTS

A. Angular dependences

The LSAW velocities were measured around the center of both the $-Z$ and $+Z$ surfaces of the specimens before and after each process to clarify the changes in the basic acoustic properties of the Z-cut LiTaO$_3$ specimens by each of the fabrication processes and as a function of the LSAW propagation direction in 1° steps at 225 MHz. Figure 2 shows the measured results after the QHT process, and Fig. 3 shows the measured results after the annealing process. In Figs. 2 and 3, 0° corresponds to the crystallographic X axis and 90° to the Y axis. The results measured for the virgin and proton-exchanged specimens are also shown in Figs. 2 and 3 for comparison. The proton exchange caused the LSAW velocities in each specimen to decrease in all the propagation directions. The angular dependences of the LSAW velocities for all the processes exhibited symmetrical cycles of 60°, reflecting the crystallographic symmetry of a Z-cut LiTaO$_3$ single crystal, and slower velocity characteristics than those
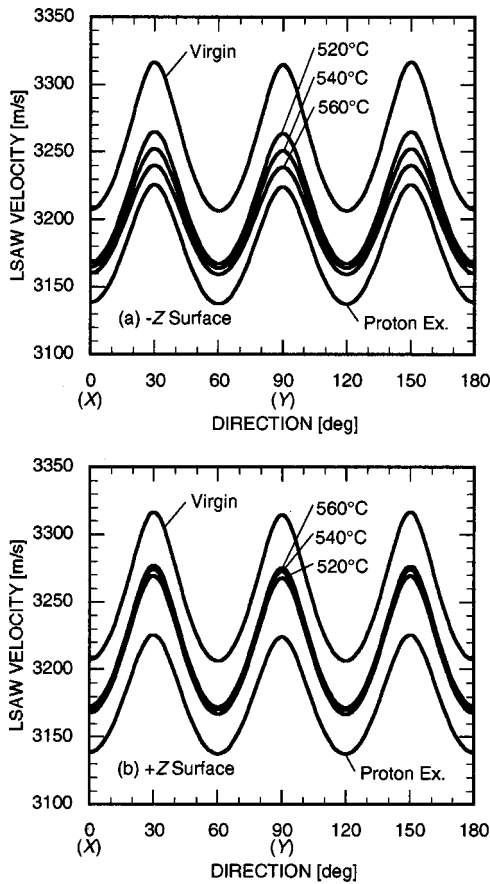
FIG. 2. Angular dependences of LSAW velocities measured for proton-exchanged and heat-treated Z-cut LiTaO$_3$ specimens at 225 MHz.
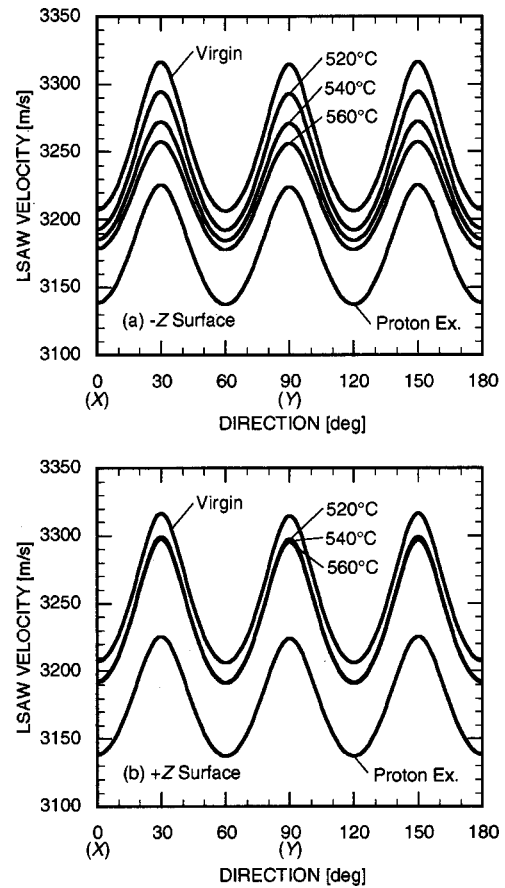

FIG. 3. Angular dependences of LSAW velocities measured for proton-exchanged, heat-treated, and annealed Z-cut LiTaO$_3$ specimens at 225 MHz.

for the virgin specimens. The changes in LSAW velocities for both the surfaces caused by all the processes were maximum in the Y-axis propagation direction and minimum in the X-axis propagation direction. The Y-axis direction is most suitable for evaluation of the fabrication process conditions of domain-inverted layers, as for evaluations of the as-proton-exchanged layers[21,24] and the proton-exchanged and annealed layers.[21,27] The changes in LSAW velocities between the processed and virgin specimens in the Y-axis direction are listed in Table I.

Figure 2 and Table I illustrate that the changes in LSAW velocities due to the proton exchange are almost the same on both surfaces. According to the literature,[24] this indicates that both surfaces are proton-exchanged under almost the same conditions and that the depths of the proton-exchanged layers formed on both surfaces are also identical. The LSAW velocities for both surfaces are increased in all the propagation directions by the QHT process. The LSAW velocities for the $-Z$ surfaces decrease significantly as the QHT temperature increases. In contrast, the LSAW velocities for the $+Z$ surfaces increase slightly as the QHT temperature increases. The LSAW velocity changes due to the QHT process depend differently on the surfaces.

The LSAW velocities for both the $-Z$ and $+Z$ surfaces further increase in all the propagation directions in Fig. 3 and Table I after the QHT and annealing processes, compared with those after the QHT process shown in Fig. 2 and Table

I. The differences in the LSAW velocities for the $-Z$ surfaces become greater depending upon the QHT temperatures. The LSAW velocities for the $+Z$ surface were always faster than those for the $-Z$ surface in each specimen, as shown in Figs. 2 and 3, and the LSAW velocities were almost the same after annealing.

B. Frequency dependences

LSAW velocities exhibit dispersion characteristics and depend on the product fH of the ultrasonic frequency f and the layer thickness H when LSAWs propagate on layered

TABLE I. Domain-inverted layer thicknesses and LSAW velocity changes for the ZY-LiTaO$_3$ specimens at 225 MHz relative to the results for the virgin specimens. Values in parentheses indicate the LSAW velocity changes by each process.

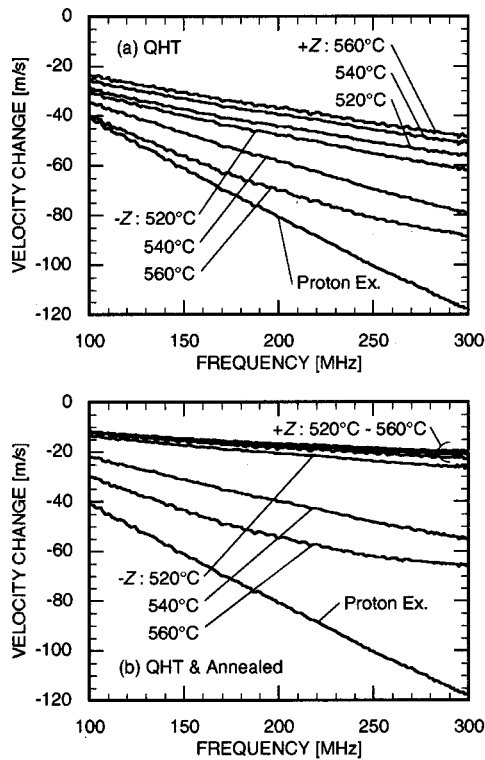| QHT temp. (°C)	Layer thickness (µm)	Surface	Differences in LSAW velocities (m/s)		
			Proton exchange	QHT	Annealing
520	0.50	−Z	−89.1	−51.2 (38.0)	−21.8 (29.4)
		+Z	−89.1	−47.1 (42.2)	−17.3 (29.8)
540	1.94	−Z	−90.5	−63.9 (26.5)	−43.9 (20.0)
		+Z	−90.4	−42.0 (48.0)	−18.0 (24.0)
560	3.26	−Z	−89.4	−75.9 (13.6)	−58.5 (17.3)
		+Z	−89.4	−39.6 (49.9)	−19.2 (20.4)

FIG. 4. Frequency dependences of LSAW velocity changes. (a) Results measured for proton-exchanged and heat-treated ZY-LiTaO$_3$ specimens. (b) Results measured for proton-exchanged, heat-treated, and annealed ZY-LiTaO$_3$ specimens.

FIG. 5. Cross-sectional photographs of domain-inverted layers formed on proton-exchanged, heat-treated, and annealed $-Z$-cut LiTaO$_3$ specimens.

media.[18,21,22,24] LSAW velocities for the Y-axis propagation were, therefore, measured before and after each process in 1-MHz steps from 100 to 300 MHz to clarify the dispersion in the specimens. Figures 4(a) and 4(b) give the results measured after QHT and after annealing. The results in the ordinate provide the LSAW velocity changes obtained by taking the differences between the processed and virgin specimens; the value of 0 m/s corresponds to an LSAW velocity of 3318 m/s on a virgin ZY-LiTaO$_3$ substrate.

The LSAW velocities for both surfaces in each specimen in Fig. 4(a) became slower as the frequency increased. The LSAW velocities for the $-Z$ surfaces are decreased by the proton exchange and increased by the QHT process, but become slower as the QHT temperature increases. The LSAW velocities for the specimens heat-treated at 520 and 540 °C decrease linearly as the frequency increases. In contrast, the gradients of the frequency dependences of the LSAW velocities for the specimen heat-treated at 560 °C become gentler with increases in the frequency. The LSAW velocities for the $+Z$ surfaces increase as the QHT temperature increases.

The LSAW velocities for both the $-Z$ and $+Z$ surfaces shown in Fig. 4(b) were increased by annealing, and the gradients of the frequency dependences became gentler. The QHT temperature dependences of the LSAW velocity frequency characteristics in the $-Z$ surfaces were similar to those before annealing, as shown in Fig. 4(a). However, the LSAW velocities became considerably faster as the QHT temperature decreased, and the differences in the LSAW velocities among the specimens became greater as the fre-
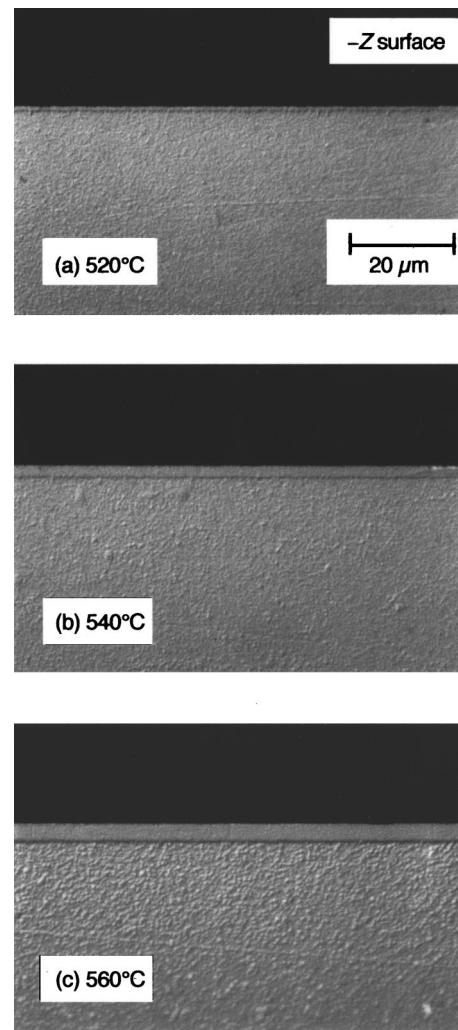
quency increased. The LSAW velocities in the $+Z$ surfaces decreased slightly with increasing frequency, and the dispersions were almost the same, independent of the QHT temperatures. The elastic properties for all the specimens are reportedly almost the same, mainly due to the annealing effect at 420 °C for 6 h.[27] These experimental results indicate that the LSAW velocities for Z-cut LiTaO$_3$ substrates with domain-inverted layers exhibit different dispersion characteristics in the $-Z$ and $+Z$ surfaces regardless of the annealing process. This implies that different surface layers on the $-Z$ and $+Z$ surfaces were formed by the proton-exchange and QHT processes.

C. Layer thickness determination

The specimens were cut along the X axis after all the processes to observe the domain-inverted layer structure and to determine the thickness. Cross-sectional $-Y$ faces that were polished and etched in a boiled mixture of HF and HNO$_3$ (2:1) for about 5 min were examined by an optical microscope.[16] Figures 5(a)–5(c) show the cross-sectional photographs of the $-Z$ surface sides for the specimens heat-treated at 520, 540, and 560 °C. The domain-inverted layers
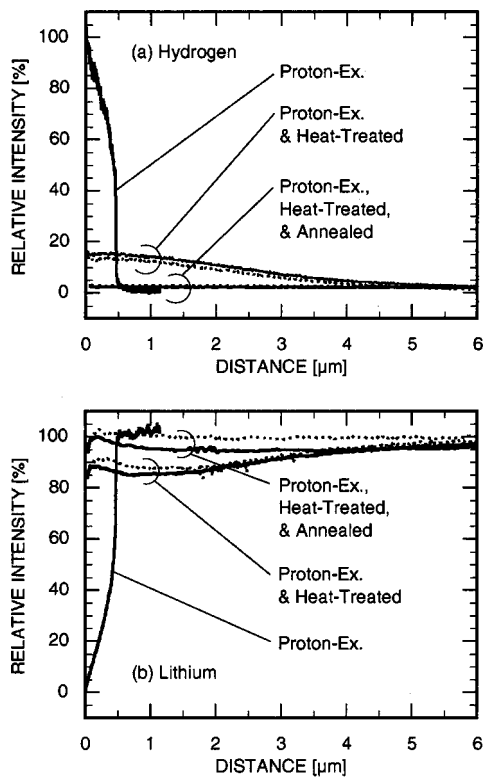
FIG. 6. Depth profiles of hydrogen and lithium ions for Z-cut LiTaO$_3$ specimens analyzed by secondary-ion mass spectrometry. Solid lines indicate the results for $-Z$ surfaces, and dotted lines, for $+Z$ surfaces of the specimens.

FIG. 7. Illustrative model of a domain-inverted layer on a minus surface side of Z-cut LiTaO$_3$ substrate proton-exchanged and QHT-processed at 540 °C. P_S: spontaneous polarization.

formed almost uniformly over the whole $-Z$ surfaces of the specimens. The thicknesses of the domain-inverted layers were estimated to be 0.50 μm at 520 °C, 1.94 μm at 540 °C, and 3.26 μm at 560 °C. The thickness error was about ±0.1 μm. The thickness increased as the temperature increased. The gradient of an approximated straight line fitted to the measured results by the least-squares method was 0.069 μm/°C.

D. Hydrogen and lithium profiles

Proton-diffused layers must be formed on both the $-Z$ and $+Z$ surfaces, since the entirety of both the $-Z$ and $+Z$ surfaces was processed without any protection masks in the proton exchange. Both surfaces of two specimens heat-treated at 540 °C with and without the annealing process are analyzed by SIMS in this section to obtain basic data about the proton-diffused layers before chemical etching to observe the domain-inverted layer structure and thicknesses in Sec. IV C. The analyzed results of depth profiles of hydrogen and lithium ions for the specimens are shown in Fig. 6. The results for the as-proton-exchanged specimen are also shown in Fig. 6 for comparison. The solid (dotted) lines in Fig. 6 represent the results for the $-Z(+Z)$ surfaces. The abscissa shows the distance from the specimen surface. The secondary-ion intensities of hydrogen in the ordinate were normalized by the intensity at the surface of the proton-exchanged specimen, and those of lithium, by the intensity around the bulk substrate region. Hydrogen ions introduced by the proton exchange diffused deeper into the substrates
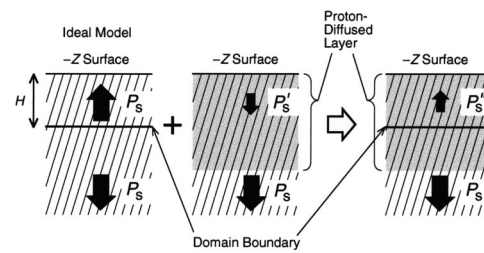
due to the QHT and annealing processes, and the relative intensities at the surfaces decreased to about 13%–14% and 2%–3%. In contrast, lithium ions diffused towards the surface from the deeper region due to the QHT and annealing, and the surface intensities increased. The depths of the proton-diffused layers, defined as the position at which the hydrogen intensity becomes $1/e$ of the surface intensity in Fig. 6, were determined to be about 0.47 ± 0.05 μm after the proton exchange, about 3.5 ± 0.3 μm after QHT, and about 21 ± 0.5 μm after annealing. The proton-diffused layer depth then became deeper, and the state in the proton-diffused layer seemed to approach the state of the original bulk substrate.

It appears in Fig. 6 that the profiles of hydrogen and lithium ions for the $-Z$ and $+Z$ surfaces differ slightly even after QHT and after annealing. The slightly different depth profiles of hydrogen and lithium ions may reflect the slight differences in the following heating conditions for the $-Z$ and $+Z$ surfaces. The $-Z$ surface was coated with Ta film and the $+Z$ surface was in contact with the graphite plate, particularly in the QHT process, as explained in Sec. III.

However, we considered the reproducibility in the SIMS measurements here and elected to assume that proton-diffused layers with almost the same depth profiles were formed on both the $-Z$ and $+Z$ surfaces of the specimens regardless of the annealing process depicted in Fig. 6. This resulted in the same wave propagation properties associated with the formation of proton-diffused layers for both surfaces.

V. DISCUSSIONS

A. Model and *fH* dependences

The experimental results in the previous section indicate that domain-inverted layers are superimposed on proton-diffused layers at the side of the $-Z$ surfaces. For example, this is illustrated in Fig. 7 for a specimen QHT-processed at 540 °C without annealing, the proton distribution for which is shown in Fig. 6(a). P_S indicates spontaneous polarization for the substrate, and its value is affected by the proton exchange and heat treatment. Thus, the LSAW velocity changes measured for the $-Z$ surfaces must include the velocity changes brought by the formation of domain-inverted layers as well as those previously reported by the formation of proton-diffused layers.[22] The results analyzed by SIMS, shown in Sec. IV D, lead us to assume that the elastic properties of the proton-diffused layers on the $-Z$ and $+Z$ sur-
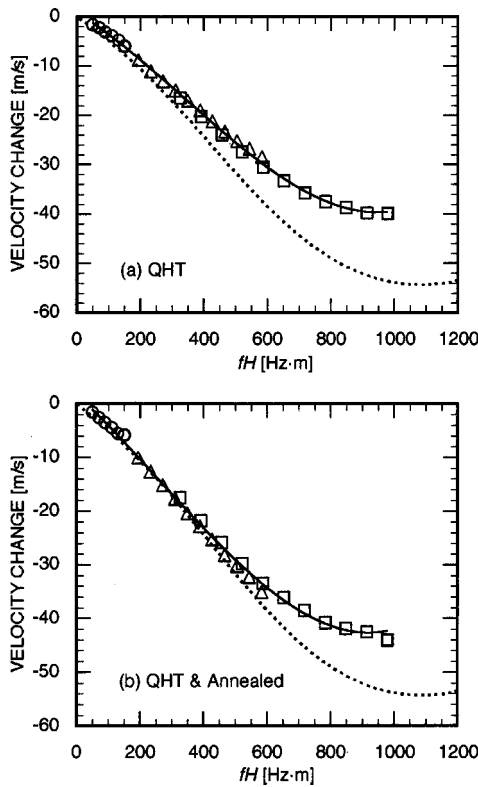
FIG. 8. fH dependences of LSAW velocity changes for ZY-LiTaO$_3$ speci-mens. Circles, triangles, and squares indicate the results measured for the specimens heat-treated at 520, 540, and 560 °C, respectively. Solid lines represent the approximated curves for the measured results, and the dotted lines are the results calculated for an ideal model of a domain-inverted layer on a Z-cut LiTaO$_3$ substrate.

faces are almost identical, since the depth profiles of hydro-gen and lithium ions in the proton-diffused layers on both the surfaces are almost the same. Therefore, intrinsic changes in LSAW velocities by the formation of domain-inverted layers could be obtained by subtracting the LSAW velocities mea-sured for the $+Z$ surfaces from those for the $-Z$ surfaces.

Figure 8 shows the fH dependences of LSAW velocities obtained by taking the differences in the LSAW velocities measured for the $-Z$ and $+Z$ surfaces of the specimens in the frequency dependences shown in Fig. 4 and using the determined layer thicknesses. Figures 8(a) and 8(b) depict the results for specimens without and with the last annealing process. The circles, triangles, and squares in Fig. 8 indicate the 6–11 values of the measured results, designated by solid lines in Fig. 4, for the specimens QHT-processed at 520, 540, and 560 °C. The LSAW velocity differences between the $-Z$ and $+Z$ surfaces monotonically decreased as fH increased and were plotted on an identical curve. Therefore, the veloc-ity differences provide information about the intrinsic veloc-ity changes only by domain inversion. It can be understood that the different LSAW velocity characteristics in Figs. 2–4, measured for the $-Z$ and $+Z$ surfaces after QHT and after annealing, were caused by the LSAW velocities decreasing as the QHT temperature was increased in a temperature range of 520–560 °C by the formation of proton-diffused layers on both surfaces and the domain-inverted layers on the $-Z$ surface. The solid lines in Figs. 8(a) and 8(b) indicate

the approximated curves obtained in the third polynomial expression that were fitted by the least-squares method to the whole measured results, given by Eqs. (2) and (3):

$$\Delta V_{LSAW} = 5.21 \times 10^{-8}(fH)^3 - 5.32 \times 10^{-5}(fH)^2$$
$$- 3.90 \times 10^{-2} fH + 0.78 \, (\text{m/s}), \quad (2)$$

$$\Delta V_{LSAW} = 4.97 \times 10^{-8}(fH)^3 - 3.88 \times 10^{-5}(fH)^2$$
$$- 5.47 \times 10^{-2} fH + 1.78 \, (\text{m/s}). \quad (3)$$

The dotted lines in Figs. 8(a) and 8(b) represent the the-oretical results numerically calculated for the LSAW propa-gation in the Y-axis direction for the ideal model of a $-Z$-cut LiTaO$_3$ substrate with a domain-inverted layer,[7,22,23] as illus-trated in Fig. 7. Only the piezoelectric constants of the acoustical physical constants (elastic constants, piezoelectric constants, dielectric constants, and density) associated with the calculations in this ideal model have signs different from those for the substrate, according to the physical constants recently reported by Kushibiki et al.[28] The calculated results exhibit the dispersion characteristics of the velocity changes of the fH dependence, revealing the differences from the ve-locity value of 3318 m/s at $fH = 0$ Hz m. This is considered to be caused by the electric-field short-circuiting effect at the domain boundary.[7] The measured results overlap and are plotted on an identical curve. Comparing the measured re-sults with the calculated results verifies that the results coin-cide well in the smaller fH range regardless of the annealing. The measured results become greater than the calculated ones as fH further increases, but the differences of LSAW velocities between the measured and calculated results are decreased remarkably by annealing. These results suggest that the differences in the measured and calculated LSAW velocities might be caused by the slightly different elastic properties for the $-Z$ and $+Z$ surfaces of the proton-diffused layers created during the QHT process, as explained in Secs. III and IV D, and the residual stresses around the domain-inverted boundary.

B. Relationships between LSAW velocity and process conditions

Setting a constant f enables us to obtain the relationship between the LSAW velocity changes and the domain-inverted layer thicknesses shown in Fig. 8. In addition, we can relate the LSAW velocity changes to the QHT process temperatures by using the relationship between the QHT pro-cess temperatures and the layer thicknesses obtained in Sec. IV C. For example, we obtain gradients of -0.0858 μm/(m/s) after QHT and -0.0782 μm/(m/s) after annealing by linear approximation using the least-squares method for the data around 540 °C for 30 s in the QHT process obtained by the LSAW velocity measurements at 225 MHz. The resolu-tion in LSAW velocity measurements around 3300 m/s 225 MHz can be estimated within ± 0.1 m/s, since the reproduc-ibility of LSAW velocity measurements is better than $\pm 0.002\%$ for $\pm 2\sigma$ (σ: standard deviation) at any chosen point.[19] Thus, the sensitivities and resolutions of the layer thicknesses and the QHT process temperatures can be calcu-lated as shown in Table II for application to thickness control

TABLE II. Sensitivity and resolution for domain-inverted layer thicknesses and QHT temperatures around 540 °C by LSAW velocity measurements.

	Annealing	LSAW velocity	Layer thickness	Process temperature
Sensitivity	No	⋯	0.0858 μm/(m/s)	1.24 °C/(m/s)
	Yes	⋯	0.0782 μm(m/s)	1.13 °C/(m/s)
Resolution	No	0.1 m/s	0.00858 μm	0.124 °C
	Yes	0.1 m/s	0.00782 μm	0.113 °C

of domain-inverted layers. The LFB-UMC system provides extremely high sensitivity and resolution for evaluation of each parameter related to the formation of domain-inverted layers.

C. Homogeneity evaluation

The homogeneities of domain-inverted layer thicknesses and their process conditions are evaluated in this section. The distributions of LSAW velocities were measured for both the $-Z$ and $+Z$ surfaces of a specimen heat-treated at 540 °C in 1-mm steps after each process of proton exchange, QHT, and annealing, and are shown as the broken line in Fig. 9(a). The differences in LSAW velocities for the surfaces were measured for the specimens after QHT and QHT and annealing at 225 MHz in the Y-axis direction to obtain information of the thickness distributions in the domain-inverted layer formed on the $-Z$ surface, as shown in Fig. 9(b). The 0-mm position corresponds to the center of the specimen. The circles in Fig. 9(b) represent the results after the QHT, and
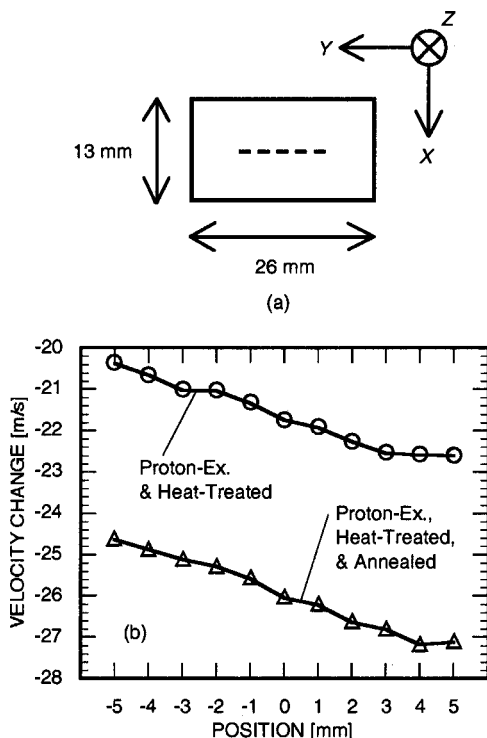

FIG. 9. Distributions of LSAW velocity changes measured at 225 MHz for the ZY-LiTaO$_3$ specimens QHT-processed at 540 °C (circles) and followed by annealing (triangles). (a) Sample configuration and (b) subtracted results of LSAW velocities between the $-Z$ and $+Z$ surfaces.
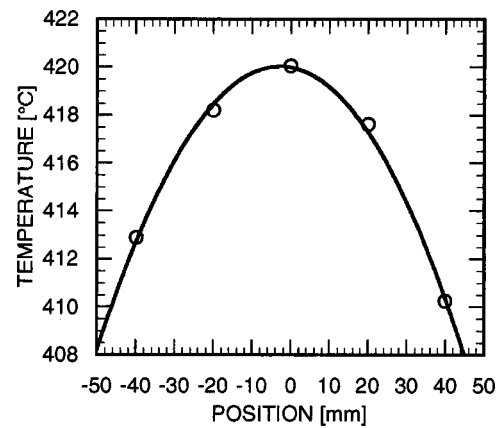

FIG. 10. Distributions of temperatures measured in the infrared ray furnace used for the QHT and annealing processes. Circles indicate the measured results, and the solid line is the approximated curve.

triangles signify the results after annealing. The velocity differences for both processes monotonically decreased with maximum deviations of 2.2 and 2.6 m/s, respectively, as the measurement positions moved from left to right. Figure 8 indicates that the differences directly reflect the distributions of layer thicknesses. The results in Table II demonstrate that the detailed thickness distributions of the domain-inverted layers could be observed with maximum deviations of 0.19 μm after the QHT process and at 0.20 μm after the annealing process, resulting in an excellent coincidence due to the superior accuracy of the system.

We measured the actual thicknesses of the domain-inverted layers at positions of -5 mm, 0 mm, and $+5$ mm by observing the cross-sectional $-Y$ faces at each position in the same manner as described in Sec. IV C. The layer thicknesses were 1.89 μm at -5 mm, 1.94 μm at 0 mm, and 1.93 μm at 5 mm. The thicknesses for the specimen were estimated to be almost uniform, with a thickness error of about ± 0.1 μm. We, therefore, considered that the major cause of the thickness distributions detected by the LSAW velocity measurements is the distribution of temperature in the QHT process, since the depth distributions of the proton-exchanged layers formed on both the surfaces were uniform. The temperature distributions in the QHT process were estimated to be about 2.9 °C within the measurement region of 10 mm, using the relationship in Table II.

For comparison, the temperature distributions in the infrared ray furnace were measured in 20-mm steps along the velocity measurement region by a thermocouple when the temperatures in the furnace were stabilized. The results are shown in Fig. 10. The position of 0 mm corresponds to the center of the furnace, which is the same position as the center of the specimen when the specimen was heated and annealed. The temperatures in the furnace were maximum around the center of the furnace and exhibited a slight asymmetry with respect to the center of the furnace. The temperature distributions in the region of -5 to $+5$ mm were estimated to be about 0.3 °C. The actual temperature distributions appeared to differ even more from the results shown in Fig. 10. They may be relatively larger than the

distributions measured in the furnace under stable temperature conditions because the specimens underwent a very fast temperature increase rate and very short soaking time in the QHT process. The LSAW velocity distributions were considered to reflect the actual temperature distributions of 2.9 °C in the QHT process, resulting in somewhat thick distributions of 0.19–0.20 μm.

VI. CONCLUDING REMARKS

In this article, we applied the LFB-UMC system to evaluate Z-cut LiTaO$_3$ substrates with domain-inverted layers and established experimental procedures to characterize and evaluate them and their fabrication process conditions. Three particular specimens with domain-inverted layers on the entire $-Z$ surfaces of Z-cut LiTaO$_3$ substrates prepared by proton exchange in a pyrophospheric acid solution, QHT, and annealing were fabricated by taking the QHT temperature as a parameter, i.e., 520, 540, and 560 °C under conditions of a temperature increase rate of 80 °C/s and short soak time of 30 s. LSAW velocity measurements were carried out for both the $-Z$ and $+Z$ surfaces of the specimens in a frequency range from 100 to 300 MHz. The angular dependences of the LSAW velocities indicated that the crystallographic Y axis was the most appropriate direction to evaluate the process conditions in the QHT, as well as those in the proton exchange and annealing, because maximum LSAW velocity changes were obtained in that direction. The LSAW velocities measured for both the $-Z$ and $+Z$ surfaces exhibited different frequency dependences. The observation of domain-inverted layers by the chemical etching technique and the depth profiles of hydrogen and lithium ions analyzed by SIMS enabled us to confirm that domain-inverted layers had formed on the $-Z$ surfaces and proton-diffused layers had formed on both the $-Z$ and $+Z$ surfaces with only slightly different depth profiles of the hydrogen and lithium ions. The LSAW velocities exhibited dispersion characteristics due to this layered structure. Intrinsic LSAW velocity changes due to the formation of domain-inverted layers were obtained by subtracting the LSAW velocities measured for the $+Z$ surfaces from those for the $-Z$ surfaces. The differences in LSAW velocities between the extracted and calculated results suggest that the domain structures in the specimens differ slightly from the ideal model of a Z-cut LiTaO$_3$ substrate with a domain-inverted layer as the fH value increases. The LSAW velocity changes were experimentally related to the layer thicknesses and the QHT temperatures. We also successfully demonstrated that homogeneities of the layer thicknesses and process conditions in the QHT process can be evaluated by LSAW velocity measurements.

Further investigations will be conducted to resolve problems associated with the differences between the measured and calculated results in the ideal domain-inverted layer structure obtained in this article and the physical property changes in the acoustic and optical properties due to the proton exchange, diffusion effects, and the annealing effect.[4,29–36] We have demonstrated the extreme usefulness of this ultrasonic method from a technical standpoint in an accurate and nondestructive examination, using the proton exchange, annealing, and domain inversion to fabricate waveguide-type optoelectronic devices, as well as single-crystal materials such as LiNbO$_3$ and LiTaO$_3$.[20,37–40] We also established experimental procedures to characterize and evaluate the fabrication techniques and the fabrication process conditions and systems. This technology can clearly be applied to evaluate other fabrication techniques of Ti-diffused layers and SiO$_2$ passivation films for waveguide-type optoelectronic devices.

[1] R. V. Schmidt and I. P. Kaminow, Appl. Phys. Lett. **25**, 458 (1974).
[2] S. Miyazawa, J. Appl. Phys. **50**, 4599 (1979).
[3] K. Nakamura, H. Ando, and H. Shimizu, *Proceedings of the IEEE Ultrasonics Symposium* (IEEE, Williamsburg, 1986), pp. 719–722.
[4] J. L. Jackel, C. E. Rice, and J. J. Veselka, Appl. Phys. Lett. **41**, 607 (1982).
[5] K. Nakamura and H. Shimizu, Appl. Phys. Lett. **56**, 1535 (1990).
[6] K. Nakamura, M. Hosoya, and A. Tourlog, J. Appl. Phys. **73**, 1390 (1993).
[7] K. Nakamura and A. Tourlog, IEEE Trans. Ultrason. Ferroelectr. Freq. Control **41**, 872 (1994).
[8] K. Nakamura and M. Itagaki, Jpn. J. Appl. Phys., Part 1 **33**, 5404 (1994).
[9] K. Nakamura, Y. Kurosawa, and K. Ishikawa, Appl. Phys. Lett. **68**, 2799 (1996).
[10] K. Nakamura and Y. Kato, IEICE Trans. **J82-C-I**, 728 (1999).
[11] W. Sohler, B. Hampel, R. Regener, R. Ricken, H. Suche, and R. Volk, J. Lightwave Technol. **4**, 772 (1986).
[12] K. Mizuuchi and K. Yamamoto, J. Appl. Phys. **72**, 5061 (1992).
[13] K. Mizuuchi, K. Yamamoto, and H. Sato, J. Appl. Phys. **75**, 1311 (1994).
[14] J. Shikata, K. Kawase, K. Karino, T. Taniuchi, and H. Ito, IEEE Trans. Microwave Theory Tech. **48**, 653 (2000).
[15] T. Hatanaka, K. Nakamura, T. Taniuchi, H. Ito, Y. Furukawa, and K. Kitamura, Opt. Lett. **25**, 651 (2000).
[16] K. Nassau, H. J. Levinstein, and G. M. Loiacono, Appl. Phys. Lett. **6**, 228 (1965).
[17] H. J. Levinstein, A. A. Ballman, and C. D. Capio, J. Appl. Phys. **37**, 4585 (1966).
[18] J. Kushibiki and N. Chubachi, IEEE Trans. Sonics Ultrason. **SU-32**, 189 (1985).
[19] J. Kushibiki, Y. Ono, Y. Ohashi, and M. Arakawa, IEEE Trans. Ultrason. Ferroelectr. Freq. Control **49**, 99 (2002).
[20] J. Kushibiki, H. Takahashi, T. Kobayashi, and N. Chubachi, Appl. Phys. Lett. **58**, 893 (1991).
[21] J. Kushibiki, M. Miyashita, and N. Chubachi, IEEE Photonics Technol. Lett. **8**, 1516 (1996).
[22] J. Kushibiki and M. Miyashita, Jpn. J. Appl. Phys., Part 2 **36**, L959 (1997).
[23] A. Tourlog, J. D. Achenbach, and J. Kushibiki, J. Appl. Phys. **81**, 6616 (1997).
[24] J. Kushibiki and M. Miyashita, J. Appl. Phys. **89**, 2017 (2001).
[25] Y. Ohashi and J. Kushibiki, Jpn. J. Appl. Phys., Part 2 **38**, L1197 (1999).

[26] J. Kushibiki and Y. Ohashi, and M. Arakawa, IEEE Trans. Ultrason. Ferroelectr. Freq. Control **47**, 274 (2000).

[27] M. Miyashita and J. Kushibiki, J. Appl. Phys. (to be published).

[28] J. Kushibiki, I. Takanaga, M. Arakawa, and T. Sannomiya, IEEE Trans. Ultrason. Ferroelectr. Freq. Control **46**, 1315 (1999).

[29] V. Hinkov and E. Ise, J. Phys. D **18**, L31 (1985).

[30] E. M. Biebl, P. H. Russer, and K. Anemogiannis, *Proceedings of the IEEE Ultrasonics Symposium* (IEEE, Montreal, 1989), pp. 281–284.

[31] Y. S. Li, K. Tada, T. Murai, and T. Yuhara, Jpn. J. Appl. Phys., Part 2 **28**, L263 (1989).

[32] M. Hirabayashi, T. Yamasaki, and Y. Komatsu, Jpn. J. Appl. Phys., Part 1 **32**, 2355 (1993).

[33] S. Kakio, J. Matsuoka, and Y. Nakagawa, Jpn. J. Appl. Phys., Part 1 **32**, 2359 (1993).

[34] J. M. Zavada, H. C. Casey, Jr., R. J. States, S. W. Novak, and A. Loni, J. Appl. Phys. **77**, 2697 (1995).

[35] T. Yuhara, K. Tada, and Y. S. Li, J. Appl. Phys. **71**, 3966 (1992).

[36] X. Cao, R. Srivastava, R. V. Ramaswamy, and J. Natour, IEEE Photonics Technol. Lett. **3**, 25 (1991).

[37] J. Kushibiki, H. Takahashi, T. Kobayashi, and N. Chubachi, Appl. Phys. Lett. **58**, 2622 (1991).

[38] J. Kushibiki, T. Kobayashi, H. Ishiji, and C. K. Jen, J. Appl. Phys. **85**, 7863 (1999).

[39] J. Kushibiki, T. Okuzawa, J. Hirohashi, and Y. Ohashi, J. Appl. Phys. **87**, 4395 (2000).

[40] J. Kushibiki, Y. Ohashi, and Y. Ono, IEEE Trans. Ultrason. Ferroelectr. Freq. Control **47**, 1068 (2000).